
CYBER MOBILITY MIRROR: DEEP LEARNING-BASED REAL-TIME 3D OBJECT PERCEPTION AND RECONSTRUCTION USING ROADSIDE LiDAR

Zhengwei Bai*, Saswat Priyadarshi Nayak, Xuanpeng Zhao, Guoyuan Wu, Matthew J. Barth

University of California, Riverside

Riverside, CA

{zbai012, snaya004, xzhao094}@ucr.edu, gywu@cert.ucr.edu, barth@ece.ucr.edu

Xuewei Qi, Yongkang Liu, Kentaro Oguchi

Toyota North America R&D Labs,

Mountain View, CA

qixuewei@gmail.com, {yongkang.liu, kentaro.oguchi}@toyota.com

ABSTRACT

Endowed with advanced wireless communication and control technologies, Connected and Automated Vehicles (CAVs) are regarded as the revolutionary promoter for Cooperative Driving Automation (CDA) to improve system operational performance. Enabling of CDA requires high-fidelity and real-time information on surrounding environment of CAVs, which is available from onboard sensors (e.g., LiDAR, camera, radar) or vehicle-to-everything (V2X) communications. Nevertheless, the accessibility of this information may suffer from the range and occlusion of perception or limited penetration rates in connectivity. In this paper, to explore the potential of roadside sensors for CDA applications in a mixed traffic environment, we introduce the prototype of *Cyber Mobility Mirror* (CMM), a next-generation real-time traffic surveillance system for 3D object detection, classification, tracking, and reconstruction, to provide CAVs with wide-range high-fidelity perception information in a mixed traffic environment. The CMM system consists of six main components: 1) the data pre-processor to retrieve and pre-process raw data from the roadside LiDAR; 2) the 3D object detector to generate 3D bounding boxes based on point cloud data; 3) the multi-objects tracker to endow unique IDs to detected objects and estimate their dynamic states; 4) the global locator to map positioning information from the LiDAR coordinate to geographic coordinate using coordinate transformation; 5) the cloud-based communicator to transmit perception information from roadside sensors to equipped vehicles; and 6) the onboard advisor to reconstruct and display the real-time traffic conditions via Graphical User Interface (GUI). In this study, a field-operational prototype system is deployed at a real-world intersection, University Avenue and Iowa Avenue in Riverside, California to assess the feasibility and performance of our CMM system. Results from field tests demonstrate that our CMM prototype system can provide satisfactory perception performance with 96.99% precision and 83.62% recall. High-fidelity real-time traffic conditions (at the object level) can be displayed on the GUI of the equipped vehicle with a frequency of 3-4 Hz.

Keywords 3D Object Detection; Multi-Object Tracking; Deep Learning; Connected and Automated Vehicles; Cooperative Driving Automation; Field Operational System.

* *Corresponding Author*

1 Introduction

With the rapid growth of travel demands, the transportation system is facing increasingly serious traffic-related challenges, such as improving traffic safety, mitigating traffic congestion, and reducing mobile source emissions. Taking advantage of recent strides in advanced sensing, wireless connectivity, and artificial intelligence, Cooperative Driving Automation (CDA) is attracting more and more attention over the past few years and is regarded as a transformative solution to the aforementioned challenges [1]. In the past few decades, several projects or programs have been conducted to explore the feasibility and potential of CDA. For instance, the California PATH program showed throughput improvement by a fully connected and automated platoon [2], and in the European DRIVE C2X project, the cooperative traffic system was assessed by large-scale field operational tests for various connected vehicle applications [3]. Recently, the U.S. Department of Transportation is leading the CARMA Program [4] for research on CDA, leveraging emerging capabilities in both connectivity and automation to enable cooperative transportation system management and operations (TSMO) strategies. Additionally, the Autonet2030 Program led by EUCar is working on Co-operative Systems in Support of Networked Automated Driving by 2030 [5].

However, most of the aforementioned projects assume an ideal scenario, i.e., all vehicles are connected and automated. Considering the fact that the presence of mixed traffic (with different types of connectivity and levels of automation) would be the norm, in the long run, one of the popular ways to enhance CAVs' adaptability in such a complicated environment is to improve their situation-awareness capability. For example, vehicles are equipped with more high-resolution onboard sensors and more powerful onboard computers to better perceive the surroundings and make decisions by themselves, a similar path to highly automated vehicles (HAVs) [6]. However, this roadmap is facing a couple of major challenges: 1) the cost of large-scale real-world implementation is prohibitive; and 2) the detection ranges are limited for onboard sensors, which also suffer from occlusion partially due to mounting heights and positions [7].

Recently, roadside sensor-assisted perception is attracting more attention for CAVs and is regarded as a promising way to unlock numerous opportunities for cooperative driving automation applications [8]. Current roadside sensing systems are mainly camera-based, which are cost-effective and well-developed for traffic surveillance such as turning movement counts, but hard to provide object-level high-fidelity 3D information caused by lighting conditions and shadowing effects [9].

Due to the capability to determine an accurate 3D location based on the point cloud, LiDAR gets more popularity in 3D object detection in traffic scenes. Previous studies validated the performance of roadside LiDAR for vehicle detection [10], vehicle tracking [11], lane identification [12], pedestrian near-crash warning [13], and other applications [14, 15]. They laid the foundation for applications with roadside LiDAR-based perception systems and unlocked more opportunities for future investigation. However, due to the lack of labeled datasets for roadside LiDARs, all these systems deploy a traditional perception pipeline [16, 17], consisting of background filtering, point cloud clustering, object classification, and object tracking. Such pipeline may generate stable results but suffers from uncertainties and generality [18]. With the development of computer vision, deep learning-based perception models show great potential to overcome the above issues.

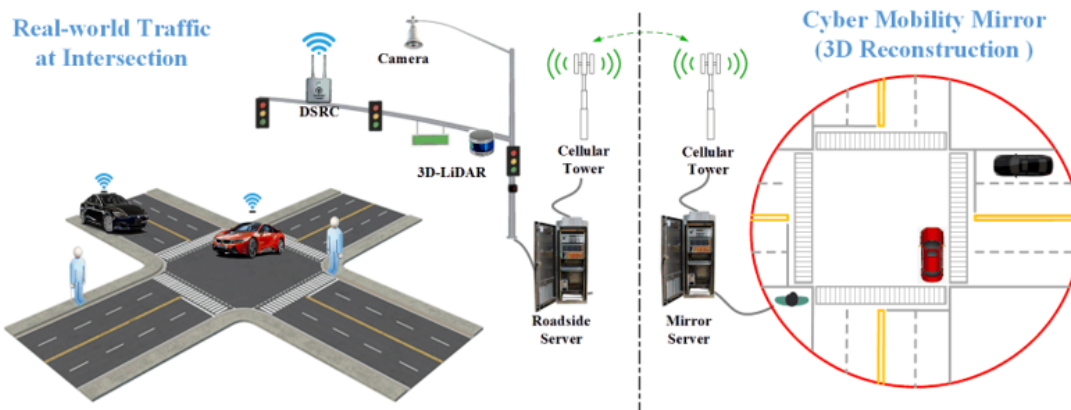


Figure 1: Illustration for CMM concept at an intersection scenario.

Nevertheless, very few studies applied deep learning-based perception algorithm to roadside LiDAR systems. To the best of the authors' knowledge, this paper is the first attempt to build a deep learning-based comprehensive 3D perception and reconstruction system for high-fidelity real-world traffic scenes. We call this system, *Cyber Mobility Mirror* or

CMM), whose key concept is shown in Fig. 1. The CMM system can perform 3D object detection, classification, tracking, and reconstruction in real-time based on 3D point cloud data from the roadside LiDAR. CAVs equipped with our CMM onboard units (OBUs) can display real-time traffic conditions at the object level on the Graphical User Interface (GUI). This high-fidelity information can serve as the stepping stone to enable various cooperative driving automation (CDA) applications.

The rest of this paper is organized as follows: related work is firstly introduced in Section 2. Section 3 shows the concept and structure of CMM, followed by the detailed description of the associated field operational system in Section 4. The results and analyses are discussed in Section 5 and the last section concludes this paper with further discussion.

2 Background

Situation awareness is one of the fundamental building blocks for Driving Automation (DA). Specifically, 3D object detection and tracking play a crucial role in perceiving the environment. Meanwhile, traffic object reconstruction helps drivers better understand the traffic conditions. Hence, in this section, related work about detection, tracking, and reconstruction for traffic objects is presented, based on a detailed literature review.

2.1 Traffic Object Detection

Object detection is a fundamental task of environment perception, and has also gone through a rapid development process in the past several decades. Back to twenty years ago, a vision-based traffic detection system made an impressive achievement using statistical methods [19]. For instance, Aslani and Mahdavi-Nasab [20] proposed an optical flow-based moving object detection method for traffic surveillance. However, these model-based methods cannot provide high fidelity detection results for more delicate applications, e.g., precise localization and object-level tracking. To explore highly accurate moving object detection methods, researchers started applying artificial neural networks [21].

With the tremendous progress of convolutional neural networks (CNNs) in vision-based tasks, CNN-based object detection methods have attracted a significant amount of attention in traffic surveillance [22]. For instance, *You Only Look Once (YOLO)* [23] and its variants, due to an impressive performance in real-time multi-object detection, get very popular in high-resolution traffic monitoring scenarios. For multi-scale vehicle object detection, Mao et al. [24] added *Spatial Pyramid Pooling (SPP)* modules in YOLO to obtain multi-resolution information. The *Single Shot MultiBox Detector (SSD)* [25] is also of significance in traffic applications. Based on SSD, Wang et al. [26] proposed a novel multi-object detection model to improve the overall perception performance under complex and wide traffic scenarios based on a multi-kernel CNN. *Faster RCNN* [27] is another generic epoch-making detection method, utilizing the region proposal ideology. To further improve the object detection performance for Faster-RCNN, Li et al. [28] proposed a cross-layer fusion structure based on Faster RCNN to achieve a nearly 10% higher average accuracy in complex traffic environments, e.g. dense traffic with shadow and occlusion.

Except the general object detection task applied in traffic scenes, many studies are conducted in terms of the special cases in traffic perception. For instance, considering that existing traffic surveillance systems were made up of costly equipment with complicated operational procedures, Mhalla et al. [29] designed an embedded computer-vision system for multi-object detection in traffic surveillance. For small object detection, Lian et al. [30] proposed an attention feature fusion block to better integrate contextual information from different layers and they were able to achieve much better performance. Targeting another edge situations, i.e. highly crowded traffic scenarios, Gahlert et al. [31] proposed the *Visibility Guided Non-Maximum Suppression (vg-NMS)* to improve the detection accuracy by leveraging both pixel-based object detection and *amodal perception* (i.e., perception of information that is common or redundant across multiple senses) paradigms. For situation awareness, Guindel et al. [32] proposed a deep CNN to jointly handle object detection and viewpoint estimation.

To support object level cooperative operations, detecting the objects in a 3D format is a straightforward and promising way for environment perception. Hence, owing to the capability to generate 3D point clouds with spatial information, it is increasingly popular for deploying 3D LiDAR to traffic environment perception. Wu et al. [10], proposed a revised *Density-Based Spatial Clustering of Applications with Noise (3D-DBSCAN)* method to detect vehicles based on roadside LiDAR sensors under rainy and snowy conditions. Using a roadside LiDAR, Zhang et al. proposed a three-stage inference pipeline, called *GC-net* [33], including the gridding, clustering, and classification. In this study, the raw point cloud data (PCD) was firstly mapped into a grid structure and then clustered by the *Grid-Density-Based Spatial Clustering* algorithm. Finally, a CNN-based classifier was applied to categorize the detected objects by extracting their local features. Liu et al. proposed a roadside LiDAR-based object detection approach by following the conventional background filtering and clustering pipeline [34], where point correlation with *KDTree* [35] neighborhood searching and adaptive Euclidean clustering were applied, respectively. To distinguish the moving object from the point cloud, Song

et al. proposed a layer-based searching method based on the feature distribution of point clouds to achieve background filtering and object detection [36]. Although 3D LiDAR has innate advantages to deal with 3D object detection, the lack of labeled roadside dataset significantly limits the potential for applying deep learning-based detectors to roadside LiDAR sensors.

2.2 Traffic Object Tracking

Deploying CDA in urban environments poses a series of difficult technological challenges out of which the object tracking is arguably one of the most significant since it provides the identification information for other subsequent technical models [37]. Object tracking can be classified into two categories in terms of the number of objects tracked at one time: one is single-object tracking (SOT) and the other is multi-object tracking (MOT). SOT has been investigated over several decades and the *Kalman filtering* methods or *particle filtering* methods have been employed widely [38, 39] for this type of tasks. For MOT tasks, some approaches have been proposed with the focus on improving accuracy and real-time performance. For instance, Bewley et al. [40] proposed *Simple Online and Real-time Tracking* (SORT) that can achieve MOT in a high frame rate without much compromising the accuracy. Based on the structure of SORT, Nicolai et al. [41] proposed a multi-object tracker – *DeepSORT*, which was capable of tracking objects with longer periods of occlusions and effectively reducing the number of identity switches by integrating the appearance features.

Considering the evolution of sensor technology and perception methods, camera-based approaches play a dominant role in traffic object tracking over the past several decades. For instance, Aslani et al. [20] applied the *Optical Flow* algorithm to detect and track moving objects by the intensity changes of frames. To improve the MOT performance, Fernandez-Sanjurjo et al. [42] built a real-time traffic monitoring system and data association with the *Hungarian* algorithm. Based on cameras equipped on an unmanned aerial vehicle (UAV), researchers [11, 43] applied correlation filters [44] to MOT tasks. Chen et al. proposed a camera-based edge traffic flow monitoring scheme using DeepSORT [45]. Recent advances in LiDAR technology enables it to hold a place in traffic object tracking tasks, by leveraging the point cloud data. For instance, Cui et al. [46] provided a simple *global nearest neighbor* (GNN) method to track multiple vehicles based on the spatial distance between consecutive frames. *Adaptive probabilistic filtering* was utilized by Kampker et al. [47] to handle uncertainties due to sensing limitations of 3D LiDARs and complexity of targets’ movements. Zhang et al., [48] used *unscented Kalman filter* (UKF) and joint probability data association filter for MOT, which improved the accuracy of estimated vehicle speed through an image matching process.

2.3 Traffic Object Reconstruction

Traffic reconstruction, traditionally, means to rebuild the traffic scenarios or parameters based on recorded sensor data, such as loop detectors and surveillance cameras [49, 50]. These traffic-level reconstruction data are valuable for macroscopic traffic management. In this paper, nevertheless, the object-level reconstruction means to rebuild the 3D location or shape of certain objects based on sensing data, which can provide visual data to support subsequent CDA applications. Several researches are conducted in this emerging area. Cao et al. [51] developed a camera-based 3D object reconstruction method in the Internet of Vehicles (IoV) environment. Rao and Chakraborty [52] proposed a LiDAR-based monocular 3D shaping to reconstruct the surrounding objects for onboard display, which has a similar purpose with the reconstruction work in this paper.

3 Cyber Mobility Mirror (CMM)

To explore the potential of the roadside sensing system, we propose a novel infrastructure-based object-level perception system, named *Cyber Mobility Mirror*. In this section, the core concept of CMM and the framework of CMM in real-world traffic environments are introduced.

3.1 Core Concept of CMM

CMM aims to enable real-time object-level traffic perception and reconstruction to empower various cooperative driving automation (CDA) applications, such as *Collision Warning* [13], *Eco-Approach and Departure* (EAD) [53], and *Cooperative Adaptive Cruise Control* (CACC) [54]. In the CMM system, traffic conditions (i.e., “mobility”) are detected by high-fidelity sensors and advanced perception methods, such as object detection, classification, and tracking. In the “cyber” world, digital replicas (i.e., “mirrored” objects) are built to reconstruct the traffic in *real-time* via high-definition 3D perception information, such as the detected objects’ geodetic locations (rendered on the satellite map), 3D dimensions, speeds, and moving directions (or headings). Then, this “mirror” can act as the perception foundation for numerous CDA applications in real-world transportation systems.

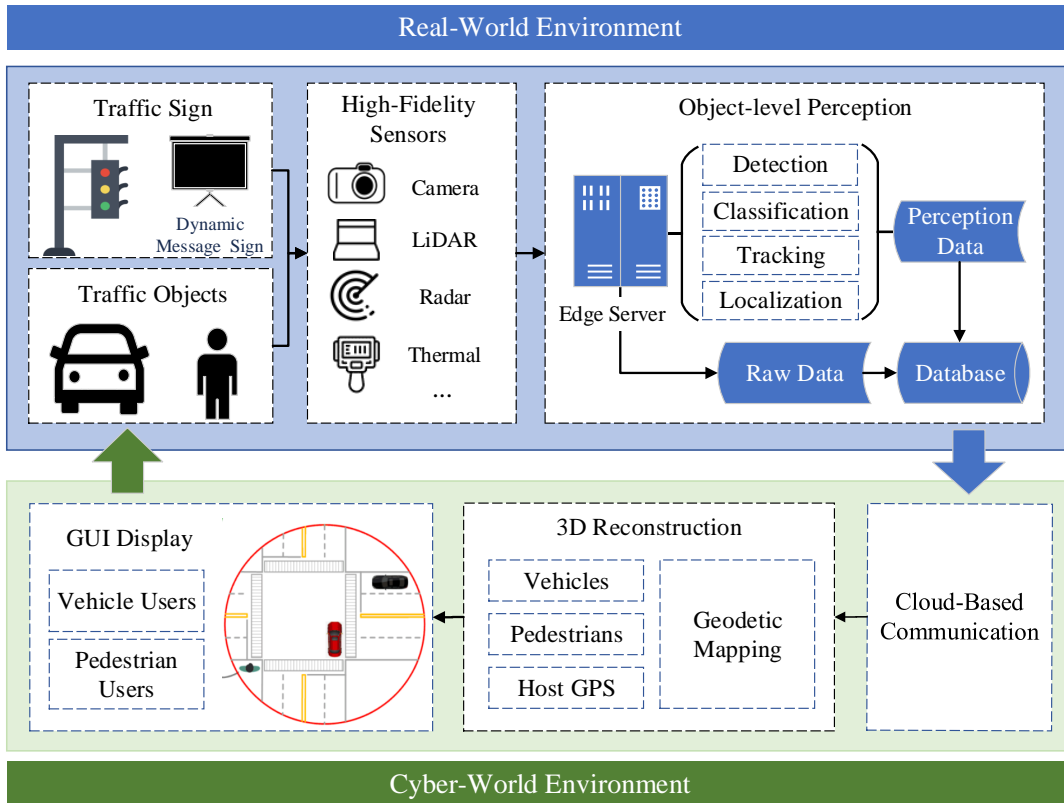


Figure 2: Systematic diagram for the core concept of CMM.

Specifically, Figure 2 illustrates the systematic diagram for the core concept of CMM. Traffic objects can be detected by high-fidelity sensors equipped at the infrastructure side and the sensing data is processed by an edge server to generate object-level information and enable various functions, such as detection, classification, tracking, and geodetic localization. The perception information is also transmitted to a cloud server for distribution and 3D reconstruction. The reconstructed traffic environment can be displayed on the GUI of connected road users to support various CDA applications. For example, in a CACC task, cooperative control or decision-making processes can be executed based on the perception of information transmitted to various traffic agents via ubiquitous connectivity [54].

3.2 Systematic Structure of CMM

In the real-world traffic environment, the system architecture of the CMM system is designed based on its core concept. Specifically, the CMM system can be divided into two main parts: the CMM Roadside System (CRS) and the CMM Onboard System (COS). Fig. 3 illustrates the system architecture and the CRS and the COS are introduced in detail as follows:

- **CMM Roadside System:** CRS consists of 1) roadside sensors, e.g., LiDAR and camera, to perceive the traffic conditions and generate high-fidelity sensor data; 2) edge computing-based real-time perception pipeline to achieve sensor fusion, object detection, classification, and tracking tasks; and 3) communication devices to receive information from other road users, infrastructure or even "clouds", and share perceived results with them via different kinds of protocols.
- **CMM Onboard System:** for CAVs, COS can receive the object-level perception data from CRS and then act as the perception inputs to support the various subsequent applications of CDA, such as CACC, cooperative merging, cooperative eco-driving; and for Connected Human-driven Vehicles (CHVs), COS can also provide them with real-time traffic information via the human-machine interface (HMI) to improve driving performance or to avoid possible crash due to the vision occlusion.

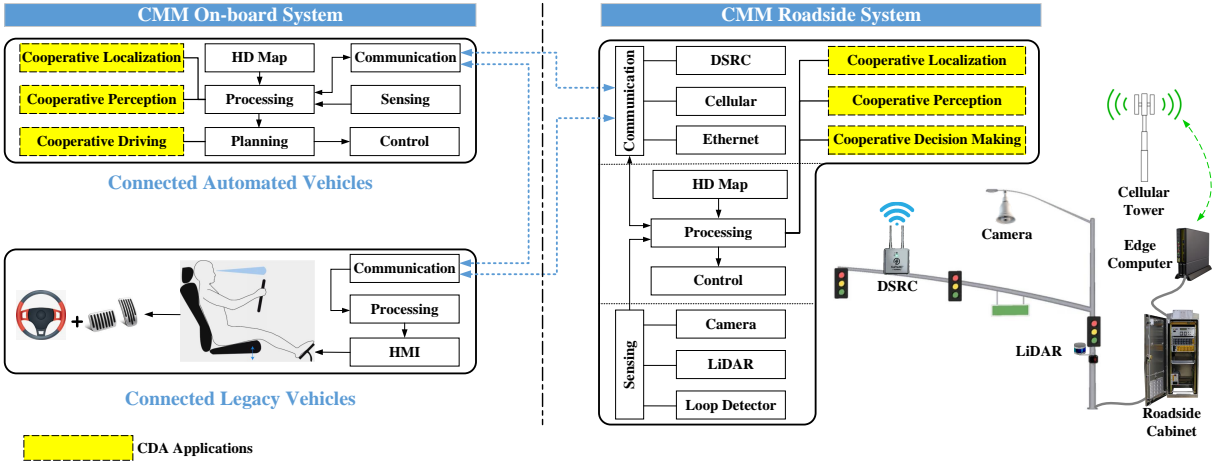


Figure 3: System structure for CMM system in Real-World Traffic Environment.

In this paper, the CMM concept is implemented in the real world and a field operational system is developed for real-world testing, which will be discussed in Section ??.

4 CMM Field Operational System

4.1 System Overview

The system overview for the CMM Field Operational System (FOS) is shown in Fig. 4. The FOS mainly consists of a roadside 3D LiDAR for data collection, an edge-computing system for data processing, a cloud server for data distribution, and a test vehicle equipped with connectivity and Graphic User Interface (GUI). To be specific, the LiDAR is installed on the signal pole high enough to achieve better coverage. The edge computer retrieves 3D point cloud data from the roadside LiDAR and then generates high-definition perception information (i.e., 3D object detection, classification, and tracking results) which is transmitted to the cloud server via Cellular Network. A CHV equipped with the CMM OBUs (including GPS receiver, onboard communication device, and a tablet) can then receive the perception information, reconstruct and display the object-level traffic condition on the GUI in real time.

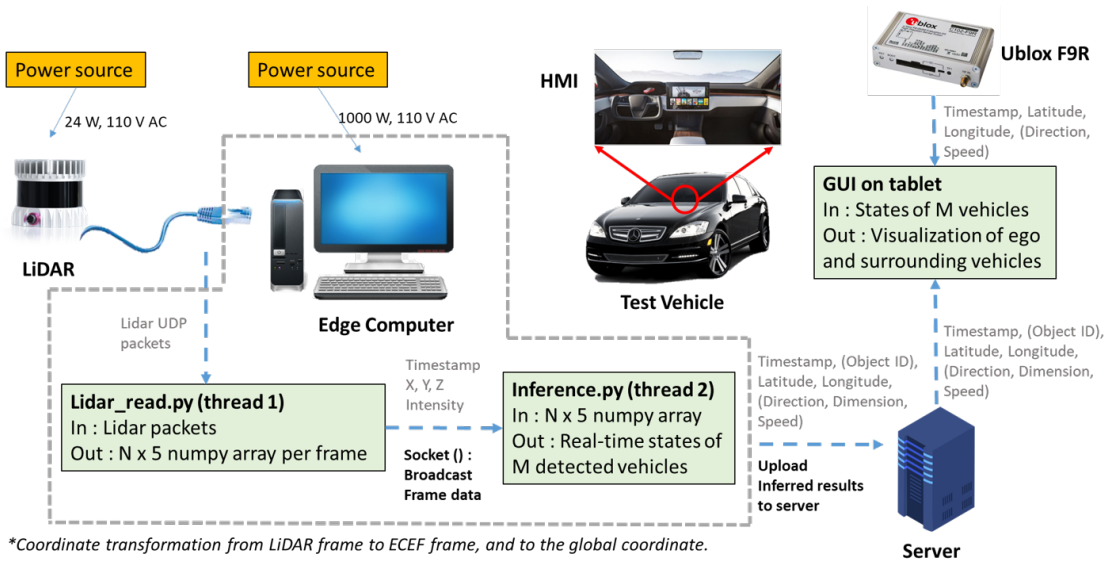


Figure 4: The architecture for CMM field operational prototype system.

4.2 System Initialization

As demonstrated by Fig. 5, the LiDAR is installed at the northwest corner of the intersection (marked as the red circle) of University Ave. and Iowa Ave. in Riverside, California. In this work, an OUSTER@64-Channel 3D LiDAR is used as a major roadside sensor, mounted on a signal pole at the height of 14-15 ft above the ground with the appropriate pitch and yaw angles to cover the monitoring area enclosed by the orange rectangle in Fig. 5. The edge computer at the intersection receives the stream of LiDAR data in the form of UDP packets. A frame of data is sampled from the incoming UDP stream. Other point cloud attributes such as 3D location, i.e., x, y, z , and the reflectivity, i , of each point are bundled into an $N \times 4$ array to be used in the inference pipeline, which will be discussed in Section 4.3.1.



Figure 5: Location and installation of the equipped roadside LiDAR.

4.3 3D Object Perception

4.3.1 Pipeline Overview

Fig. 6 shows the systematic diagram for the 3D object perception pipeline, which consists of five main sub-processes as follows:

- **Data Retrieving and Pre-processing:** collecting data from the LiDAR, converting it to a certain format, and recording it in real-time;
- **3D Object Detection:** generating rotated 3D bounding boxes by utilizing PointPillars [56];
- **Multi-Object Tracking:** endowing each traffic object with a unique ID based on DeepSORT [57];
- **Georeferencing:** converting position data from the Horizontal Coordinate to the Geodetic Coordinate (i.e., latitude, longitude, altitude);
- **Message Encoding:** encoding perception information into a certain data format for the message transmission.

These sub-processes are designed based on different algorithms to solve specific signal processing tasks. To establish a real-time operational system, several adjustments are applied to each sub-process particularly, which will be discussed in detail successively as follows.

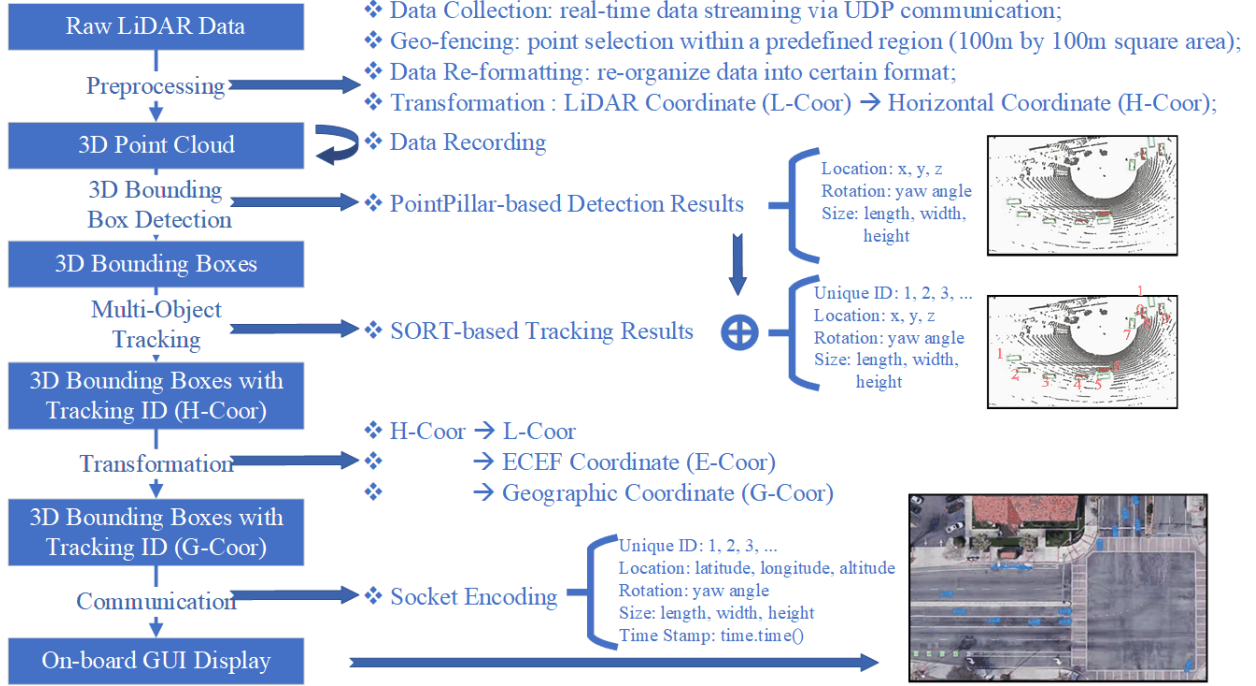


Figure 6: Systematic diagram for the perception pipeline.

4.3.2 Data Retrieving and Preprocessing

The raw point cloud data is generated by a 64-channel 3D LiDAR and then the edge computer retrieves the raw data through an Ethernet cable via UDP communication. In this paper, the detection range Ω for the roadside LiDAR is defined as a $102.4m \times 102.4m$ area centered on the location of LiDAR. The raw point cloud data can be described by:

$$\mathcal{P} = \{[x, y, z, i]^T \mid [x, y, z]^T \in \mathbb{R}^3, i \in [0.0, 1.0]\} \quad (1)$$

Then, \mathcal{P} is geo-fenced by:

$$\mathcal{P}_\Omega = \{[x, y, z, i]^T \mid x \in [-51.2m, 51.2m], y \in [-51.2m, 51.2m], z \in [-5.0m, 0m], i \in [0.0, 1.0]\} \quad (2)$$

where \mathcal{P}_Ω represent the 3D point cloud data after geo-fencing. Since ground truth labels are collected according to the objects within the target range, we choose $z \in [-5.0m, 0m]$, considering the calibrated Lidar z position of $4.74m$. Thus the detection range can cover an area above the ground to about $5.0m$ height, expecting trucks as the highest objects.

Considering the LiDAR's limited vertical field of view (FOV), we installed it with adjusted rotation angle, i.e., pitch, yaw, and roll, to cover the desired surveillance area as shown in Fig 7. Since we do not label the dataset collected from our roadside LiDAR, a pretrained 3D object detection method is implemented which is trained based on data from a horizontal installed LiDAR [58]. Hence, to mitigate the impact of the difference from settings between different LiDARs, the geo-fenced data \mathcal{P}_Ω are transformed from LiDAR Coordinate (L-Coor) to the Horizontal LiDAR coordinate (H-Coor). To achieve the exact rotation information for the real-world LiDAR, we apply a self-calibration method to generate the calibration matrix \mathcal{P}_{Cali} for the roadside LiDAR. Then the \mathcal{P}_{Cali} is implemented to transform the coordinates of 3D points from LiDAR Coordinate to Horizontal LiDAR Coordinate. The transformation process is described by Eq. 3 and visualized in Fig 7.

$$\mathcal{P}_H = \mathcal{P}_{Cali} \cdot \mathcal{P}_\Omega \quad (3)$$

4.3.3 3D Object Detection

For 3D object detection, one of the SOTA algorithms for LiDAR-based detection, PointPillar [56] is applied in our framework. Dozens of 3D object detection algorithms are tried for our roadside LiDAR data, but few of them can generate valid results. A hypothesis is that all the existing models are trained with the datasets collected from onboard LiDARs (e.g., KITTI [59], nuScenes [58]) whose configuration parameters (e.g., mounting height, pitch, yaw) are quite

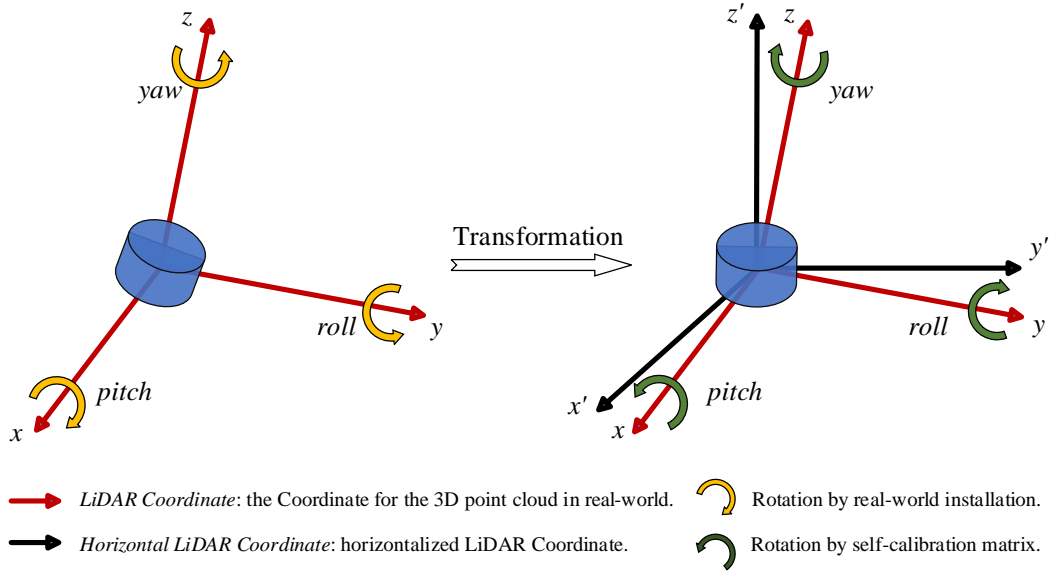


Figure 7: Description for the initial transformation for LiDAR point cloud data.

different from those of roadside LiDARs. Although coordinate transformation can be applied to potentially reduce such disparities, a better way is to identify a data representation method that is more robust to the LiDAR configuration parameters such as mounting height. Owing to the capability of data aggregation along the z -axis, i.e., the perspective of height, PointPillar can generate the most satisfying results among the methods we tested and that's the main reason that we chose PointPillar as our core detection method.

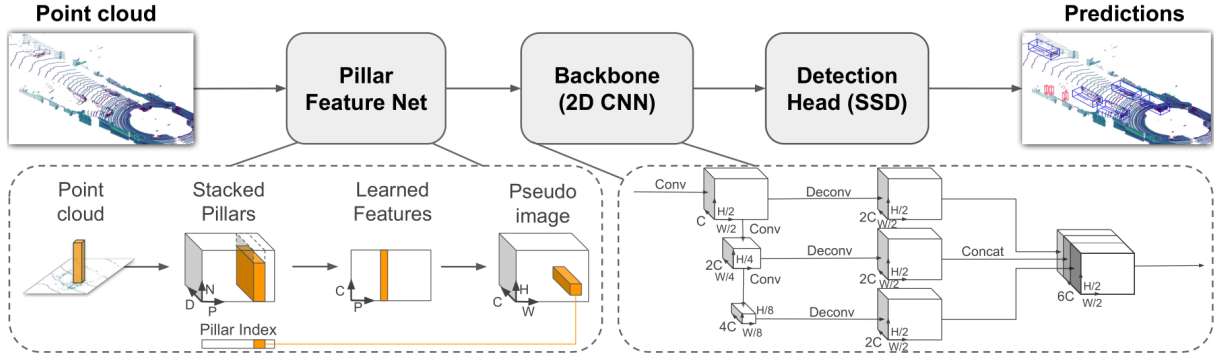


Figure 8: Network overview for the PointPillar [56].

Fig. 8 shows the network structure of the PointPillar. The main innovation is the Pillar Feature Net (PFT), which can generate a pseudo image based on the pillar-wise information of the 3D point cloud. After the PFT, a feature pyramid network (FPN) is applied and connected by the Single Shot Multi-box Detector (SSD) [25] detection head. In this work, loss functions are applied based on the SECOND [60]. Ground truth boxes and anchors are defined by a 8-dimensional vector $(x, y, z, w, l, h, \theta)$. The localization regression residuals between ground truth and anchors are defined by:

$$\Delta x = \frac{x^{gt} - x^a}{d^a}, \Delta y = \frac{y^{gt} - y^a}{d^a}, \Delta z = \frac{z^{gt} - z^a}{h^a}, \quad (4)$$

$$\Delta w = \log \frac{w^{gt}}{w^a}, \Delta l = \log \frac{l^{gt}}{l^a}, \Delta h = \log \frac{h^{gt}}{h^a}, \quad (5)$$

$$\Delta\theta = \sin(\theta^{gt} - \theta^a) \quad (6)$$

where the superscript gt and a represent the ground truth and anchor, respectively, and d^a is defined by:

$$d^a = \sqrt{(w^a)^2 + (l^a)^2}. \quad (7)$$

The total localization loss is:

$$\mathcal{L}_{loc} = \sum_{b \in (x, y, z, w, l, h, \theta)} \text{SmoothL1}(\Delta b) \quad (8)$$

Inspired by [60], a softmax classification loss, \mathcal{L}_{dir} , is used to distinguish flipped boxes. The object classification is enabled by the focal loss [61], which is shown as:

$$\mathcal{L}_{cls} = -\alpha_a (1 - p^a)^\gamma \log p^a, \quad (9)$$

where p^a is the class probability of an anchor and the α and β are set as the same as the original paper. Hence, the total loss is:

$$\mathcal{L} = \frac{1}{N_{pos}} (\beta_{loc} \mathcal{L}_{loc} + \beta_{cls} \mathcal{L}_{cls} + \beta_{dir} \mathcal{L}_{dir}), \quad (10)$$

where N_{pos} is the number of positive anchors and β_{loc} , β_{cls} and β_{dir} are set as 2, 1, and 0.2.

4.3.4 3D Multi-Object Tracking

To build a real-world system, time delay and computational requirements are important factors. DeepSORT, due to its satisfactory performance in a high frame rate with low computational resources, is adapted in our CMM FOS for multi-object tracking (MOT). However, the original DeepSORT is mainly defined for MOT on image data, i.e. the 2D object tracking, and is not compatible with object detection with 3D bounding boxes. Thus, we design an enhanced DeepSORT, named 3D DeepSORT, which can resolve objects with 3D locations. To be specific, 2D location information is filtered from the 3D detection results and the 2D location data will be fed into the DeepSORT model to generate the 2D MOT results, i.e. unique identification (ID) number for each object. Then, a Euclidean distance-based data matching algorithm is designed to generate the enhanced 3D MOT results. Algorithm 1 demonstrates the details.

Algorithm 1 The description for 3D DeepSORT.

Input: The instant 3D object detection results: $Dboxes = \{D^{(i)}(x, y, z, w, l, h, \theta) | i = 1, 2, \dots, N_{Dbbx}\}$;

Output: The multi-object tracking results: $Tboxes = \{T^{(i)}(x, y, z, w, l, h, \theta, id) | i = 1, 2, \dots, N_{Dbbx}\}$;

```

1: function 3D DEEPSORT( $Dboxes$ )
2:    $Dboxes_{2d} \leftarrow D^{(i)}(x, y, w, l) | i = 1, 2, \dots, N_{Dbbx}$ ;
3:    $Tboxes_{2d} = \{T_{2d}^{(j)}(x, y, w, l, id) | j = 1, 2, \dots, N_{Tbbx}\} \leftarrow \text{DeepSORT}(Dboxes_{2d})$ ;
4:   for  $Dboxes_{2d}^{(i)} \in Dboxes_{2d}$  do
5:     for  $Tboxes_{2d}^{(j)} \in Tboxes_{2d}$  do
6:       if Euclidean distance of  $(Dboxes_{2d}^{(i)}, Tboxes_{2d}^{(j)}) < d_o$  then
7:          $T^i \leftarrow [D^{(i)}, Tboxes_{2d}(id)]$ ; Continue;
8:       end if
9:     end for
10:  end for
11:   $Tboxes = \{T^{(i)} | i = 1, 2, \dots, N_{Dbbx}\}$ 
12:  return  $Tboxes$ ;
13: end function

```

where N_{Dbbx} and N_{Tbbx} are the numbers of the detection bounding boxes and 2D tracking boxes from DeepSORT. Additionally, id represents the tracking identification number for each unique object.

4.3.5 Geo-localization

To endow the perception data with more generality, the geo-referencing of the point cloud is developed in this work. However, the output T_{boxes} from the 3D MOT is calculated based on the Horizontal-LiDAR Coordinate, i.e. a Cartesian Coordinate centered with the sensor installed evenly. Thus, the input of the geo-localization data, i.e. the T_{boxes} from Algorithm 1, is then fed into several transformation processes to transform the object location information to Geodetic Coordinate, i.e. latitude, longitude, and altitude. There are three transformations: 1) from the horizontal-LiDAR coordinate to the real LiDAR coordinate; 2) from the real LiDAR coordinate to the Geocentric Earth-centered Earth-fixed (ECEF) coordinate; and 3) from ECEF coordinate to the geodetic coordinate (i.e., latitude, longitude, and altitude). Specifically, the World Geodetic System 1984 (WGS84) is applied for the geo-transformation. The transformation from the Horizontal LiDAR coordinate to the ECEF coordinate system is shown as Eq. 11.

$$\begin{bmatrix} X_{ecef} \\ Y_{ecef} \\ Z_{ecef} \\ 1 \end{bmatrix} = \mathcal{P}_{ECEF} \cdot \mathcal{P}_{Cali}^{-1} \cdot \begin{bmatrix} X_{hor} \\ Y_{hor} \\ Z_{hor} \\ 1 \end{bmatrix} \quad (11)$$

where $\mathcal{P}_{Cali}^{-1} \in \mathcal{R}^{4 \times 4}$ and $\mathcal{P}_{ECEF} \in \mathcal{R}^{4 \times 4}$ are the inverse of the LiDAR calibration matrix, and the ECEF transformation matrix, respectively. X_{hor} , Y_{hor} , and Z_{hor} represent the coordinates of 3D points with respect to Horizontal LiDAR Coordinate. The \mathcal{P}_{ECEF} matrix responsible for transforming points in LiDAR coordinate frame to the geocentric coordinate frame (ECEF) is calculated using the Ground Control Point surveying technique [62].

The longitude (λ) is calculated from the ECEF position using the Eq. 12,

$$\lambda = \arctan\left(\frac{Y_{ecef}}{X_{ecef}}\right) \quad (12)$$

The geodetic latitude (ϕ) is calculated using Bowring's method by solving Eq. 13 and Eq. 14 in an iterative manner,

$$\bar{\beta} = \arctan\left(\frac{Z_{ecef}}{(1-f)s}\right) \quad (13)$$

$$\bar{\phi} = \arctan\left(\frac{Z_{ecef} + e^2\left(\frac{1-f}{1-e^2}\right)R(\sin\beta)^3}{s - e^2R(\cos\beta)^3}\right) \quad (14)$$

where R , f , and $e^2 = 1 - (1-f)^2$ are the equatorial radius, flattening of the planet, and the square of first eccentricity, respectively. s is defined as $s = \sqrt{X_{ecef}^2 + Y_{ecef}^2}$. The altitude (h_{ego} , height above ellipsoid) is given by,

$$h_{ego} = s \cos \phi + (Z_{ecef} + e^2 N \sin \phi) \sin \phi - N \quad (15)$$

where N , the radius of curvature in the vertical prime, is defined as

$$N = \frac{R}{\sqrt{1 - e^2(\sin \phi)^2}} \quad (16)$$

Then the geo-referenced perception information (ϕ , λ , h_{ego}) along with other data will be transmitted to the cloud server for distribution and the final data is packaged as:

$$Data_{roadside} = \{M^{(i)}(t, id, \phi, \lambda, h_{ego}, w, l, h, \theta) | i = 1, 2, \dots, N_{Dbbx}\} \quad (17)$$

4.4 Multi-Objects Reconstruction

4.4.1 Cloud Communication

As shown in Fig 9, onboard units (OBUs) retrieve traffic perception data from the cloud server and GPS location data from a GPS receiver. Then the onboard unit reconstructs the traffic conditions based on the multi-source data and displays it on the graphical user interface (GUI) in real time (the update frequency is 3-4 Hz on average). In our field implementation, a Samsung Galaxy Tab A7 tablet serves as an OBU, running a designed application to retrieve data

from the GPS receiver and display the reconstructed object-level traffic information on the GUI. We adopt a NETGEAR AirCard 770S mobile hotspot which is equipped with a 4G/LTE sim card and can provide V2C communication between the cloud server and the onboard unit. To have accurate GPS measurements, we utilize a C102-F9R U-Blox unit with an embedded Inertial Measurement Unit (IMU) which provides an 8Hz update frequency on the GPS location and heading.

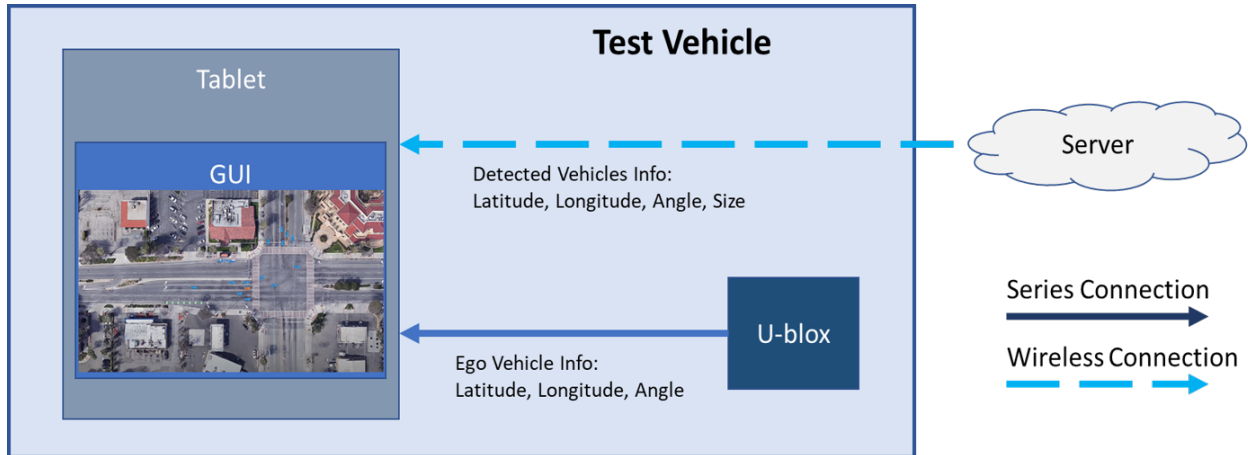


Figure 9: Illustration of onboard settings (structure and communications).

4.4.2 Reconstruction

An application is designed to visualize the location of vehicles perceived by the roadside unit (RSU) and the ego vehicle provided by the OBU. To achieve that, we first locate the monitored area at the intersection and crop it from the Google Earth Pro satellite view. We leverage the cropped image as a background map for visualizing the reconstructed traffic. Then we define two cross-referenced points: one is a GPS coordinate point on the map while the other is a pixel coordinate point on the tablet’s screen. With these two GPS coordinates, we convert the latitude and longitude of them into two-dimensional distance coordinates. Based on the pixel difference between the two reference points and the calculated vertical and horizontal direction distance difference, we can calculate the transfer ratio between them. By now, we can create an object and display it on the desired pixel coordinates based on its GPS location.

For the rest of this section, we divide them into two parts based on the information source: u-blox, and cloud server. As mentioned, u-blox can provide an 8Hz update frequency on the GPS location and heading of the ego vehicle. The tablet and the u-blox are wire-connected and the data is transmitted via Universal Serial Bus (USB) serial connection between them. With the GPS location and heading, the ego vehicle is displayed on the GUI as an orange vehicle model. On the other hand, the data from the cloud server contains the perception information, including GPS location, heading, and size of three-dimension, obtained from the RSU. From the cloud server data, we first separate the vehicle data from the pedestrian data based on the three-dimensional size information. Then display the vehicles sensed by the RSU with blue vehicle icons and pedestrians with pedestrian top view icons.

5 Field Testing and Results Analysis

5.1 Feasibility

Object-level perception information acts as the building blocks for CMM, which requires high-fidelity data retrieved from different types of high-resolution sensors, such as cameras and LiDARs. Nevertheless, it could be costly, time-consuming, and to some extent, restricted by policies and protocols, to deploy these sensors directly in the real world. Thus, it is necessary to evaluate the feasibility of the system at the early stage of this work.

To find an efficient and cost-effective way to validate the feasibility of CMM, we emulated a CMM system in a simulation platform, i.e., a CARLA-based co-simulation system [63], before the real-world implementation. As demonstrated in Fig. 10, the basic idea is to emulate the real-world traffic environment via one CARLA simulator [64] and run the entire perception process within the emulated real-world environment. Then the other CARLA simulator is applied to emulate the cyber world, i.e., to reconstruct the traffic objects and then display them. Owing to the capability of CARLA to model high-fidelity sensors, the evaluation results of the emulated CMM in the co-simulation platform can lay the foundation for real-world CMM implementation.

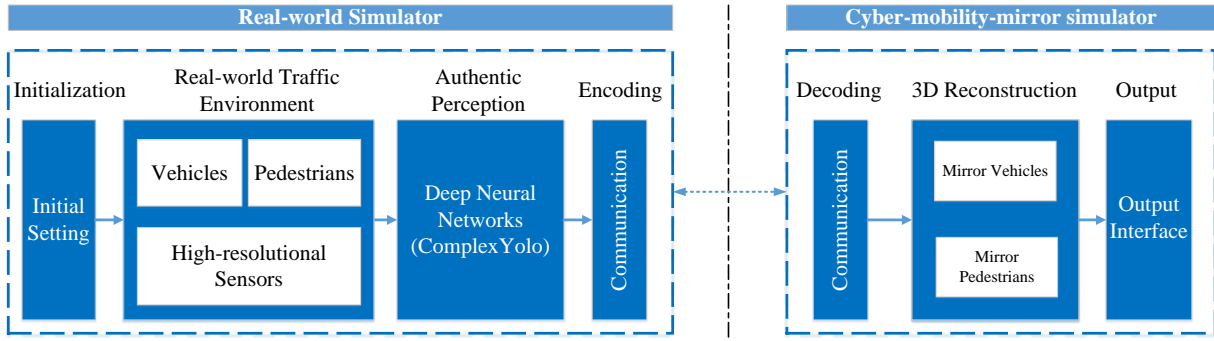


Figure 10: Structure for the CMM-based co-simulation platform.

After the feasibility check in the simulation environment, we implement the CMM field operational system (FOS) at a real-world intersection of University Ave. & Iowa Ave. in Riverside, California. Fig. 11 depicts the field system from different views. Multi-view videos are captured along the test including drone’s view, in-vehicle views (including driver perspective, backseat passenger perspective, and GUI), roadside view, and point cloud data-based bird’s-eye view (BEV). A video clip is edited with the descriptive annotations to show the whole online process, which is available at: <https://www.youtube.com/watch?v=0egpmgkzyG0>. The video demonstrates the feasibility of the CMM FOS and the following sections will show the results of detection accuracy and real-time performance.

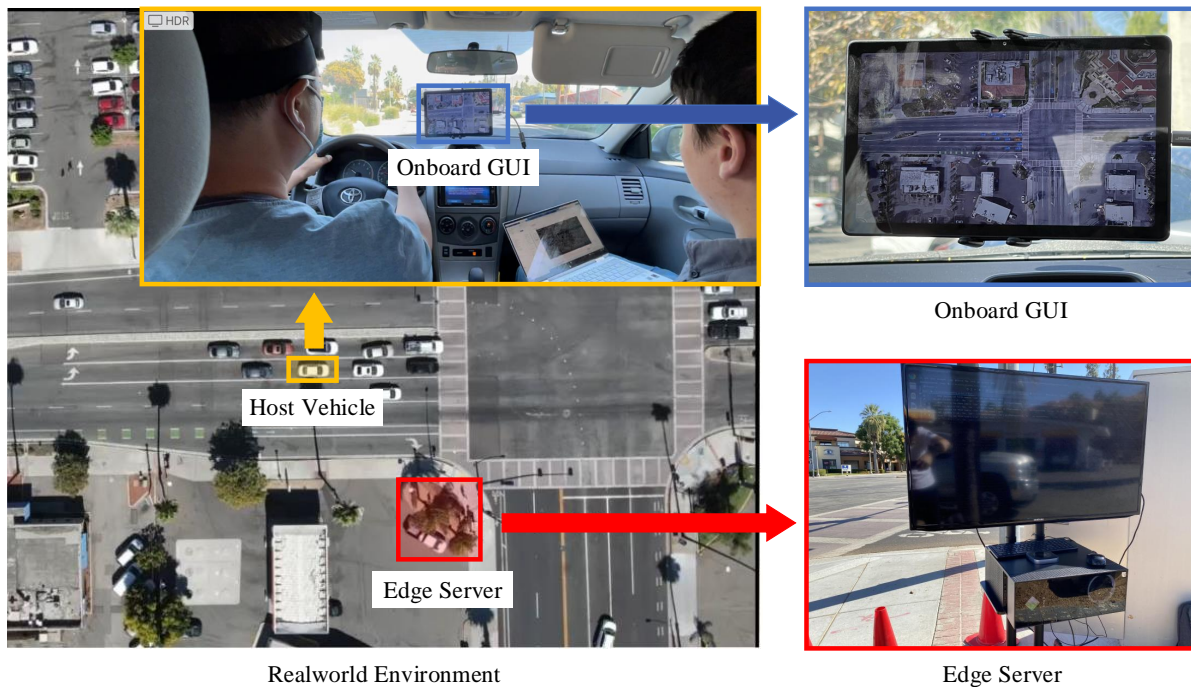
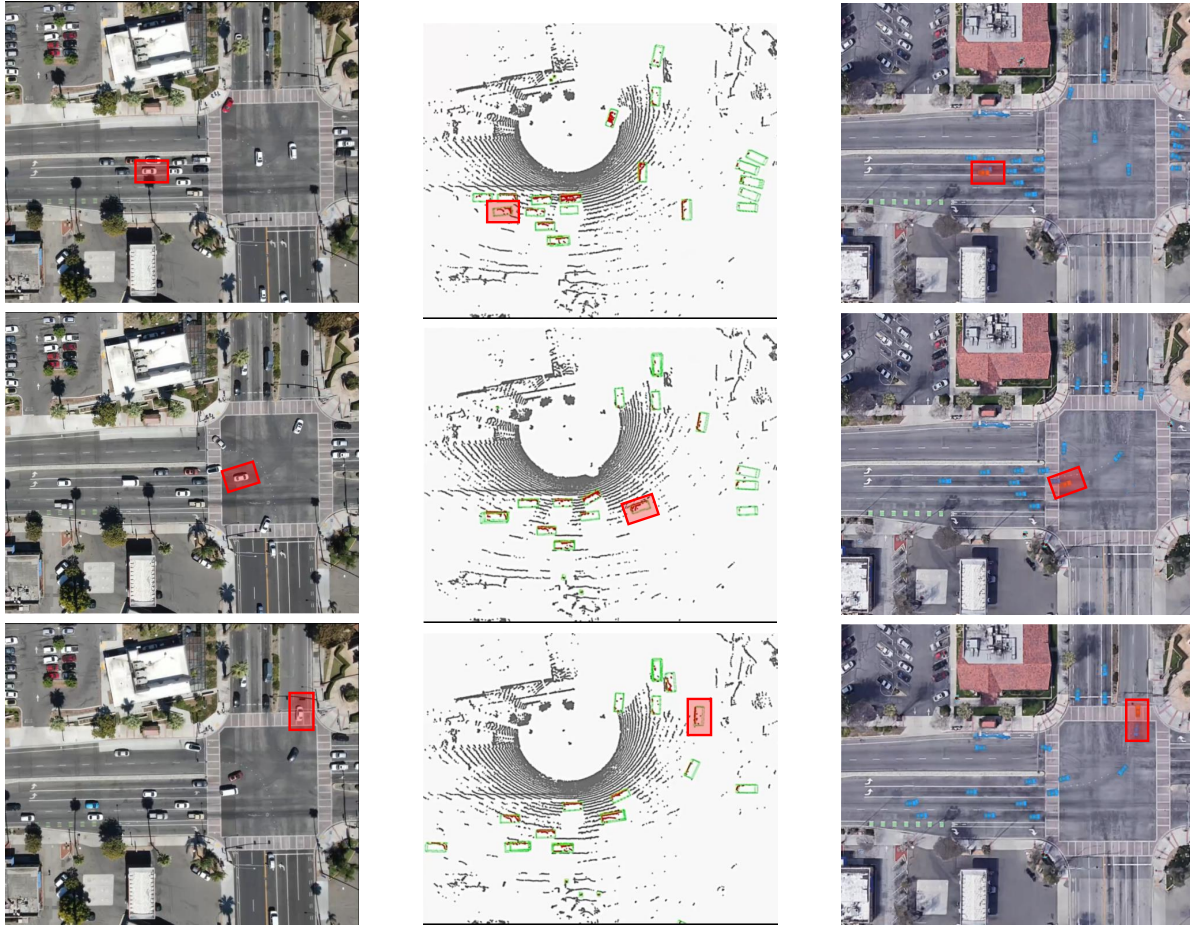


Figure 11: Illustration of CMM field operational test from different views from a drone, host vehicle, onboard GUI, and edge server.

5.2 Detection Performance

Figure 12 demonstrates several frames of the CMM FOS testing results. The first column shows the drone view, the second column depicts the bird’s-eye view from LiDAR data, and the third column presents the reconstructed view on the onboard graphical user interface. The ego vehicle equipped with the CMM onboard system is marked by a red



(a) Ground Truth (The Drone's View). (b) Visualization of 3D Bounding Boxes. (c) Reconstruction on GUI.

Figure 12: Examples of the CMM FOS testing results from different perspectives: (a) the ground truth, (b) 3D detection results, and (c) reconstruction results. The host vehicle equipped with our CMM onboard system is marked by red boxes.

rectangle in each figure. In the GUI, the orange icons represent the GPS locations of the ego vehicle, while the blue ones denote vehicles detected by the roadside LiDAR. Additionally, pedestrians are also detected and shown in the GUI with top view pedestrian icons (shown in the video). It is worth mentioning that the tracking results are generated and transmitted to the onboard side but are not further explored in this current version of CMM system. Meanwhile, due to the lack of labeled datasets, only detection accuracy is evaluated by the confusion matrix, a popular evaluation process used in the computer vision area [65].

Specifically, the detection results can be categorized into four classes, which are:

- **True Positive (TP):** the number of cases predicted as positive by the classifier when they are indeed positive, i.e., a vehicle object is detected as a vehicle.
- **False Positive (FP)** = the number of cases predicted as positive by the classifier when they are indeed negative, i.e., a non-vehicle object is detected as a vehicle.
- **True Negative (TN)** = the number of cases predicted as negative by the classifier when they are indeed negative, i.e., a non-vehicle object is detected as a non-vehicle object.
- **False Negative (FN)** = the number of cases predicted as negative by the classifier when they are indeed positive, i.e., a vehicle is detected as a non-vehicle object.

Precision is the ability of the detector to identify only relevant objects, i.e., vehicles and pedestrians in this paper. It is the proportion of correct positive predictions and is given by

$$Precision = \frac{TP}{TP + FP} = \frac{TP}{\# \text{ of all detections}} \quad (18)$$

Recall is a metric that measures the ability of the detector to find all the relevant cases (that is, all the ground-truths). It is the proportion of true positive detected among all ground-truth (i.e., real vehicles) and is defined as

$$Recall = \frac{TP}{TP + FN} = \frac{TP}{\# \text{ of all ground truth}} \quad (19)$$

In terms of the perspective for traffic surveillance, we define another metric named *Miss* which measures the portion of “missing” vehicles (that are not detected) and is defined by

$$Miss = \frac{FN}{TP + TN} = \frac{\# \text{ of all missing vehicles}}{\# \text{ of all ground truth}} \quad (20)$$

To evaluate the prototype system performance, we randomly select 130 frames of testing data and manually label them based on the drone’s view. A total of 1661 vehicles are labeled as the ground truth and the detection accuracy is evaluated based on the three aforementioned parameters. Table 1 summarizes the evaluation results.

Table 1: Test performance of CMM FOS

Ground Truth	TP	FP	Precision	Recall	Miss
1661	1389	43	96.99%	83.62%	16.38%

5.3 Latency

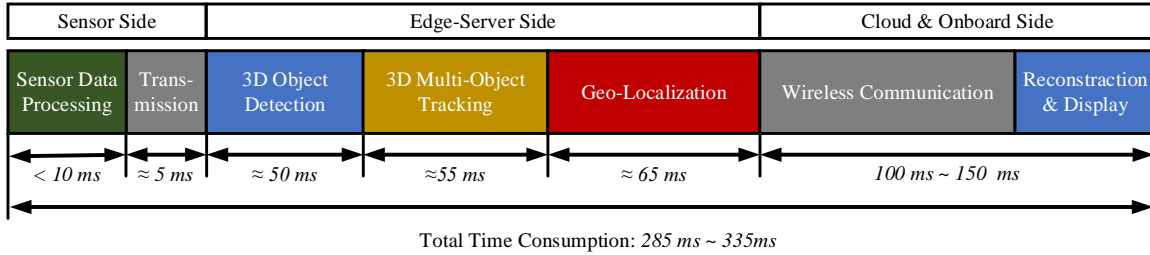


Figure 13: Visualization for the latency on account of different processes in CMM FOS.

As for a real-time FOS, it is of great significance to analyze the latency of the whole system. Depicted by Fig 13, the latency of the whole CMM FOS pipeline can be analyzed by breaking down the whole workflow into three main phases:

- **Phase 1 – Sensor Side:** Time elapsed from the moment happens till the edge server receives the sensor data. Specifically, in the *sensor processing* stage, the sensor collects the raw data and processes it into a transformable format via its embedded system. For data retrieving, the processed data can be transmitted to the edge server via Local Area Network (LAN). The time consumption is collected from the official Datasheets of OUSTER.
- **Phase 2 – Edge-Server Side:** Time elapsed from the sensor data received by the edge server till the perception data is encoded and sent out to the cloud server. The edge server is responsible for generating the object-level perception data, including 3D object detection, 3D multi-object tracking, and geodetic localization. Since these modules are running in chronological order, the time consumption for each module is measured by the starting and ending timestamps of each function.
- **Phase 3 – Cloud & Onboard Side:** Time elapsed from the perception data is sent from the edge server till the reconstructed traffic environments are displayed on the onboard GUI. Since the CMM system tends to serve all the road users with connectivity, a cloud server is involved in the data acquisition, synchronization, and distribution of processed data (after edge computing). The onboard computer, i.e. the tablet utilized in this study, will then decode the perception data, reconstruct the traffic environment, and display it on the GUI. Time consumption for this phase is measured by the timestamps from the onboard end and the edge-server end.

As shown in Fig 13, the total latency is about $285ms - 335ms$, whose variance is mainly resulted from the fluctuation of communication. However, during the field testing, we find that the time consumption of every single computational module may vary within a different fluctuation range. For example, the object-tracking and geo-localization modules have a larger variance compared with the object detection model, which may be caused by the change of the number of detected objects. The actual computational time is varying from $250ms - 335ms$ per frame, i.e., $3Hz - 4Hz$ running frequency.

To reduce the latency of the whole system, there are several ways that can be applied in the future. For example, several *for loops* and *external python packages* are implemented in the software for tracking and localization parts which mainly account for the surprisingly high computational cost at the perception end. So programming optimization can be applied in this part to squeeze out more computational time. Another strength forward way to speed up the whole process is to improve the hardware computational performance for edge server and onboard computer.

6 Conclusion and Discussion

In this study, we introduce the concept of Cyber Mobility Mirror (CMM) and develop a CMM Field Operational System at a real-world intersection as a prototype for enabling Cooperative Driving Automation (CDA). It leverages high-fidelity roadside sensors (e.g., LiDAR) to detect, classify, track and reconstruct object-level traffic information in real time, which can lay a foundation of environment perception for various kinds of CDA applications in mixed traffic. Testing results prove the feasibility of the CMM concept and also demonstrate satisfactory system performance in terms of real-time high-fidelity traffic detection and reconstruction. The overall perception accuracy metrics include 96.99% for precision and 83.62% for recall at a real-time running frequency of 3-4 Hz.

Based on this prototype CMM FOS, several future directions for improving the system performance may include:

- **Perception Accuracy:** The performance of the detection method applied in this study is limited by the lack of customized training datasets. Since it is a cost-effective way to collect training datasets from the SOTA autonomous driving simulators, e.g., CARLA [64], we will improve the detection accuracy by enhancing the model with transferability, i.e., training on simulation and testing on real-world;
- **Perception Range:** The current CMM FOS only involves one LiDAR sensor and thus can only cover near-half of the intersection area. To extend the perception range of the CMM system, we plan to set up several sensors including both LiDARs and cameras to cover multiple intersections to achieve a corridor-level cooperative perception system;
- **Real-time Performance:** The time consumption can be mainly reduced from the edge-server side, i.e., optimizing the software programming in the tracking and localization parts. Besides, upgrading the hardware equipment can also improve the real-time processing speed.

This paper intends to provide a prototype field operational system of a novel concept of roadside sensor-based perception system, named CMM, which hopes can provide foundations and inspirations for future work. By leveraging the high-fidelity roadside sensing information available from the CMM system, plenty of subsequent CDA applications (e.g., CACC, advanced intersection management, cooperative eco-driving) can be revisited for real-world implementation in the mixed traffic environment.

Acknowledgments

This research was funded by the Toyota Motor North America InfoTech Labs. The contents of this paper reflect the views of the authors, who are responsible for the facts and the accuracy of the data presented herein. The contents do not necessarily reflect the official views of Toyota Motor North America.

References

- [1] Daniel J Fagnant and Kara Kockelman. Preparing a nation for autonomous vehicles: opportunities, barriers and policy recommendations. *Transportation Research Part A: Policy and Practice*, 77:167–181, 2015.
- [2] James A Misener and Steven E Shladover. Path investigations in vehicle-roadside cooperation and safety: A foundation for safety and vehicle-infrastructure integration research. In *2006 IEEE Intelligent Transportation Systems Conference*, pages 9–16. IEEE, 2006.
- [3] R Stahlmann, A Festag, A Tomatis, I Radusch, and F Fischer. Starting european field tests for car-2-x communication: the drive c2x framework. In *18th ITS World Congress and Exhibition*, page 12, 2011.

- [4] USDOT. Carma program overview, May 2021.
- [5] EUCAR. Autonet2030, May 2021.
- [6] Eduardo Arnold, Omar Y Al-Jarrah, Mehrdad Dianati, Saber Fallah, David Oxtoby, and Alex Mouzakitis. A survey on 3d object detection methods for autonomous driving applications. *IEEE Transactions on Intelligent Transportation Systems*, 20(10):3782–3795, 2019.
- [7] Ekim Yurtsever, Jacob Lambert, Alexander Carballo, and Kazuya Takeda. A survey of autonomous driving: Common practices and emerging technologies. *IEEE access*, 8:58443–58469, 2020.
- [8] Zhengwei Bai, Guoyuan Wu, Xuewei Qi, Yongkang Liu, Kentaro Oguchi, and Matthew J Barth. Infrastructure-based object detection and tracking for cooperative driving automation: A survey. *arXiv preprint arXiv:2201.11871*, 2022.
- [9] Sokemi Rene Emmanuel Datondji, Yohan Dupuis, Peggy Subirats, and Pascal Vasseur. A survey of vision-based traffic monitoring of road intersections. *IEEE transactions on intelligent transportation systems*, 17(10):2681–2698, 2016.
- [10] Jianqing Wu, Hao Xu, Jianying Zheng, and Junxuan Zhao. Automatic vehicle detection with roadside lidar data under rainy and snowy conditions. *IEEE Intelligent Transportation Systems Magazine*, 13(1):197–209, 2020.
- [11] Junxuan Zhao, Hao Xu, Hongchao Liu, Jianqing Wu, Yichen Zheng, and Dayong Wu. Detection and tracking of pedestrians and vehicles using roadside lidar sensors. *Transportation research part C: emerging technologies*, 100:68–87, 2019.
- [12] Jianqing Wu, Hao Xu, and Junxuan Zhao. Automatic lane identification using the roadside lidar sensors. *IEEE Intelligent Transportation Systems Magazine*, 12(1):25–34, 2018.
- [13] Jianqing Wu, Hao Xu, Yongsheng Zhang, and Renjuan Sun. An improved vehicle-pedestrian near-crash identification method with a roadside lidar sensor. *Journal of safety research*, 73:211–224, 2020.
- [14] Zhenyao Zhang, Jianying Zheng, Hao Xu, Xiang Wang, Xueliang Fan, and Rong Chen. Automatic background construction and object detection based on roadside lidar. *IEEE Transactions on Intelligent Transportation Systems*, 21(10):4086–4097, 2019.
- [15] Bin Lv, Hao Xu, Jianqing Wu, Yuan Tian, Yongsheng Zhang, Yichen Zheng, Changwei Yuan, and Sheng Tian. Lidar-enhanced connected infrastructures sensing and broadcasting high-resolution traffic information serving smart cities. *IEEE Access*, 7:79895–79907, 2019.
- [16] Yanjie Song, Han Zhang, Yuanqiang Liu, Jinzhang Liu, Hongbo Zhang, and Xiuguang Song. Background filtering and object detection with a stationary lidar using a layer-based method. *IEEE Access*, 8:184426–184436, 2020.
- [17] Martin Ester, Hans-Peter Kriegel, Jörg Sander, Xiaowei Xu, et al. A density-based algorithm for discovering clusters in large spatial databases with noise. In *kdd*, volume 96, pages 226–231, 1996.
- [18] Zhengxia Zou, Zhenwei Shi, Yuhong Guo, and Jieping Ye. Object detection in 20 years: A survey. *arXiv preprint arXiv:1905.05055*, 2019.
- [19] Rita Cucchiara, Costantino Grana, Metal Piccardi, and A Prati. Statistic and knowledge-based moving object detection in traffic scenes. In *ITSC2000. 2000 IEEE Intelligent Transportation Systems. Proceedings (Cat. No. 00TH8493)*, pages 27–32. IEEE, 2000.
- [20] Sepehr Aslani and Homayoun Mahdavi-Nasab. Optical flow based moving object detection and tracking for traffic surveillance. *International Journal of Electrical, Computer, Energetic, Electronic and Communication Engineering*, 7(9):1252–1256, 2013.
- [21] Shih-Chia Huang and Bo-Hao Chen. Highly accurate moving object detection in variable bit rate video-based traffic monitoring systems. *IEEE transactions on neural networks and learning systems*, 24(12):1920–1931, 2013.
- [22] Azzedine Boukerche and Zhijun Hou. Object detection using deep learning methods in traffic scenarios. *ACM Computing Surveys (CSUR)*, 54(2):1–35, 2021.
- [23] Joseph Redmon, Santosh Divvala, Ross Girshick, and Ali Farhadi. You only look once: Unified, real-time object detection. In *Proceedings of the IEEE conference on computer vision and pattern recognition*, pages 779–788, 2016.
- [24] Qi-Chao Mao, Hong-Mei Sun, Ling-Qun Zuo, and Rui-Sheng Jia. Finding every car: a traffic surveillance multi-scale vehicle object detection method. *Applied Intelligence*, 50(10):3125–3136, 2020.
- [25] Wei Liu, Dragomir Anguelov, Dumitru Erhan, Christian Szegedy, Scott Reed, Cheng-Yang Fu, and Alexander C Berg. Ssd: Single shot multibox detector. In *European conference on computer vision*, pages 21–37. Springer, 2016.

- [26] Xinqing Wang, Xia Hua, Feng Xiao, Yuyang Li, Xiaodong Hu, and Pengyu Sun. Multi-object detection in traffic scenes based on improved ssd. *Electronics*, 7(11):302, 2018.
- [27] Shaoqing Ren, Kaiming He, Ross Girshick, and Jian Sun. Faster r-cnn: Towards real-time object detection with region proposal networks. *Advances in neural information processing systems*, 28:91–99, 2015.
- [28] Cui-jin Li, Zhong Qu, Sheng-ye Wang, and Ling Liu. A method of cross-layer fusion multi-object detection and recognition based on improved faster r-cnn model in complex traffic environment. *Pattern Recognition Letters*, 145:127–134, 2021.
- [29] Ala Mhalla, Thierry Chateau, Sami Gazzah, and Najoua Essoukri Ben Amara. An embedded computer-vision system for multi-object detection in traffic surveillance. *IEEE Transactions on Intelligent Transportation Systems*, 20(11):4006–4018, 2018.
- [30] Jing Lian, Yuhang Yin, Linhui Li, Zhenghao Wang, and Yafu Zhou. Small object detection in traffic scenes based on attention feature fusion. *Sensors*, 21(9):3031, 2021.
- [31] Nils Gähler, Niklas Hanselmann, Uwe Franke, and Joachim Denzler. Visibility guided nms: Efficient boosting of amodal object detection in crowded traffic scenes. *arXiv preprint arXiv:2006.08547*, 2020.
- [32] Carlos Guindel, David Martin, and Jose Maria Armingol. Fast joint object detection and viewpoint estimation for traffic scene understanding. *IEEE Intelligent Transportation Systems Magazine*, 10(4):74–86, 2018.
- [33] Liwen Zhang, Jianying Zheng, Rongchuan Sun, and Yanyun Tao. Gc-net: Gridding and clustering for traffic object detection with roadside lidar. *IEEE Intelligent Systems*, 2020.
- [34] Zihan Liu, Qizhong Li, Shengming Mei, and Miaohua Huang. Background filtering and object detection with roadside lidar data. In *2021 4th International Conference on Electron Device and Mechanical Engineering (ICEDME)*, pages 296–299, 2021.
- [35] Stephen J Redmond and Conor Heneghan. A method for initialising the k-means clustering algorithm using kd-trees. *Pattern recognition letters*, 28(8):965–973, 2007.
- [36] Yanjie Song, Han Zhang, Yuanqiang Liu, Jinzhang Liu, Hongbo Zhang, and Xiuguang Song. Background filtering and object detection with a stationary lidar using a layer-based method. *IEEE Access*, 8:184426–184436, 2020.
- [37] SAE. Taxonomy and definitions for terms related to cooperative driving automation for on-road motor vehicles j3216_202005. Available: https://www.sae.org/standards/content/j3216_202005/, 2021.
- [38] Erik V Cuevas, Daniel Zaldivar, and Raul Rojas. Kalman filter for vision tracking. 2005.
- [39] Kenji Okuma, Ali Taleghani, Nando De Freitas, James J Little, and David G Lowe. A boosted particle filter: Multitarget detection and tracking. In *European conference on computer vision*, pages 28–39. Springer, 2004.
- [40] Alex Bewley, Zongyuan Ge, Lionel Ott, Fabio Ramos, and Ben Upcroft. Simple online and realtime tracking. In *2016 IEEE international conference on image processing (ICIP)*, pages 3464–3468. IEEE, 2016.
- [41] Nicolai c, Alex Bewley, and Dietrich Paulus. Simple online and realtime tracking with a deep association metric. In *2017 IEEE International Conference on Image Processing (ICIP)*, pages 3645–3649, 2017.
- [42] Mauro Fernandez-Sanjurjo, Brais Bosquet, Manuel Mucientes, and Victor M Brea. Real-time visual detection and tracking system for traffic monitoring. *Engineering Applications of Artificial Intelligence*, 85:410–420, 2019.
- [43] Navaneeth Balamuralidhar, Sofia Tilon, and Francesco Nex. Multeye: Monitoring system for real-time vehicle detection, tracking and speed estimation from uav imagery on edge-computing platforms. *Remote Sensing*, 13(4):573, 2021.
- [44] David S Bolme, J Ross Beveridge, Bruce A Draper, and Yui Man Lui. Visual object tracking using adaptive correlation filters. In *2010 IEEE computer society conference on computer vision and pattern recognition*, pages 2544–2550. IEEE, 2010.
- [45] Chen Chen, Bin Liu, Shaohua Wan, Peng Qiao, and Qingqi Pei. An edge traffic flow detection scheme based on deep learning in an intelligent transportation system. *IEEE Transactions on Intelligent Transportation Systems*, 22(3):1840–1852, 2020.
- [46] Yuepeng Cui, Hao Xu, Jianqing Wu, Yuan Sun, and Junxuan Zhao. Automatic vehicle tracking with roadside lidar data for the connected-vehicles system. *IEEE Intelligent Systems*, 34(3):44–51, 2019.
- [47] Achim Kampker, Mohsen Sefati, Arya S Abdul Rachman, Kai Kreisköther, and Pascual Campoy. Towards multi-object detection and tracking in urban scenario under uncertainties. In *VEHITS*, pages 156–167, 2018.
- [48] Jiaxing Zhang, Wen Xiao, Benjamin Coifman, and Jon P Mills. Vehicle tracking and speed estimation from roadside lidar. *IEEE Journal of Selected Topics in Applied Earth Observations and Remote Sensing*, 13:5597–5608, 2020.

- [49] Juan C Herrera and Alexandre M Bayen. Traffic flow reconstruction using mobile sensors and loop detector data. 2007.
- [50] Dingde Jiang, Wenjuan Wang, Lei Shi, and Houbing Song. A compressive sensing-based approach to end-to-end network traffic reconstruction. *IEEE Transactions on Network Science and Engineering*, 7(1):507–519, 2018.
- [51] Mingwei Cao, Liping Zheng, Wei Jia, and Xiaoping Liu. Joint 3d reconstruction and object tracking for traffic video analysis under iov environment. *IEEE Transactions on Intelligent Transportation Systems*, 22(6):3577–3591, 2021.
- [52] Qing Rao and Samarjit Chakraborty. In-vehicle object-level 3d reconstruction of traffic scenes. *IEEE Transactions on Intelligent Transportation Systems*, pages 1–13, 2020.
- [53] Zhengwei Bai, Peng Hao, Wei Shangguan, Baigen Cai, and Matthew J. Barth. Hybrid reinforcement learning-based eco-driving strategy for connected and automated vehicles at signalized intersections. *IEEE Transactions on Intelligent Transportation Systems*, pages 1–14, 2022.
- [54] Ziran Wang, Yougang Bian, Steven E. Shladover, Guoyuan Wu, Shengbo Eben Li, and Matthew J. Barth. A survey on cooperative longitudinal motion control of multiple connected and automated vehicles. *IEEE Intelligent Transportation Systems Magazine*, 12(1):4–24, 2020.
- [55] MMDetection3D Contributors. MMDetection3D: OpenMMLab next-generation platform for general 3D object detection. <https://github.com/open-mmlab/mmdetection3d>, 2020.
- [56] Alex H Lang, Sourabh Vora, Holger Caesar, Lubing Zhou, Jiong Yang, and Oscar Beijbom. Pointpillars: Fast encoders for object detection from point clouds. In *Proceedings of the IEEE/CVF Conference on Computer Vision and Pattern Recognition*, pages 12697–12705, 2019.
- [57] Xinyu Hou, Yi Wang, and Lap-Pui Chau. Vehicle tracking using deep sort with low confidence track filtering. In *2019 16th IEEE International Conference on Advanced Video and Signal Based Surveillance (AVSS)*, pages 1–6. IEEE, 2019.
- [58] Holger Caesar, Varun Bankiti, Alex H Lang, Sourabh Vora, Venice Erin Liong, Qiang Xu, Anush Krishnan, Yu Pan, Giancarlo Baldan, and Oscar Beijbom. nuscenes: A multimodal dataset for autonomous driving. In *Proceedings of the IEEE/CVF conference on computer vision and pattern recognition*, pages 11621–11631, 2020.
- [59] Andreas Geiger, Philip Lenz, and Raquel Urtasun. Are we ready for autonomous driving? the kitti vision benchmark suite. In *Conference on Computer Vision and Pattern Recognition (CVPR)*, 2012.
- [60] Yan Yan, Yuxing Mao, and Bo Li. Second: Sparsely embedded convolutional detection. *Sensors*, 18(10):3337, 2018.
- [61] Tsung-Yi Lin, Priya Goyal, Ross Girshick, Kaiming He, and Piotr Dollár. Focal loss for dense object detection. In *Proceedings of the IEEE international conference on computer vision*, pages 2980–2988, 2017.
- [62] Sara Schuhmacher and Jan Boehm. Georeferencing of terrestrial laserscanner data for applications in architectural modeling. 2005.
- [63] Zhengwei Bai, Guoyuan Wu, Xuwei Qi, Kentaro Oguchi, and Matthew J Barth. Cyber mobility mirror for enabling cooperative driving automation: A co-simulation platform. *arXiv preprint arXiv:2201.09463*, 2022.
- [64] Alexey Dosovitskiy, German Ros, Felipe Codevilla, Antonio Lopez, and Vladlen Koltun. Carla: An open urban driving simulator. In *Conference on robot learning*, pages 1–16. PMLR, 2017.
- [65] Mark Everingham, SM Eslami, Luc Van Gool, Christopher KI Williams, John Winn, and Andrew Zisserman. The pascal visual object classes challenge: A retrospective. *International journal of computer vision*, 111(1):98–136, 2015.